*34th EPS Conference on Plasma Phys. Warsaw, 2 - 6 July 2007 ECA Vol.**31F**, P-2.020 (2007)*

Variation of the midplane heat flux width with plasma current and heating power in NSTX

R. Maingi[a] and the NSTX Team

[a] *Oak Ridge National Laboratory*

Introduction

Spherical tokamaks (ST) are often designed as high power density systems, owing to modest major radius and high plasma current (I_p) relative to higher aspect ratio tokamaks. The high plasma current is fully utilized at sufficiently high heating power to reach the β limit, resulting in substantial heat flux to the divertor components. Hence the divertor power loading is thought to be one of the main challenges of future ST devices, particularly as power levels increase to the design values in component test facilities[1].

The outer divertor peak heat flux in the National Spherical Torus Experiment (NSTX) has reached 10 MW/m^2 in certain cases[2], and heat flux peak and width scaling with control parameters is an important component of the NSTX boundary physics program for projection to future devices. Previously it was shown[3] that the peak heat flux increased strongly with neutral beam injection (NBI) power and I_p, and that the divertor profile width decreased with I_p. The profiles exhibit a steep gradient near the separatrix, and a shallower gradient farther in the scrape-off layer (SOL), as commonly observed in many tokamaks. The focus of this paper is on the midplane scale length of the steep gradient region, which extends typically for 2-3 decay lengths. The decay length of the profiles is assessed following mapping to the midplane, and compared with several models in the literature. We note that NSTX studies of heat flux management and mitigation are discussed in other publications[4-6].

Summary of experiment and measurement technique

The experiment has been described in previous papers[3, 7], and is summarized briefly here. The discharges were conducted in lower single-null (LSN) diverted configuration, with a typical poloidal flux expansion ~ 5 between the midplane and target. The magnetic balance parameter δ_r^{sep}, the distance between the dominant X-point and second X-point mapped to the outer midplane, was typically between 1.2 and 1.5 cm. These discharges had the following parameters: $0.6 \le I_p \le 0.9$ MA, $2 \le P_{NBI} \le 6$ MW, toroidal field on-axis B_t=0.45 T, elongation κ=2.0, average triangularity δ~0.45, and a large inner-wall gap between 6 and 10 cm. Neutral beam heating during the I_p ramp was used to minimize volt-second consumption and extend the pulse length. As in many NSTX H-mode discharges, the density ramped with time, owing partly to continuous gas fueling from the high-field side gas injector which improves the reliability of H-mode access in STs[8, 9]. Discharges with a short quasi-steady phase were restricted to two time slices, whereas up to 6 separate time slices were analyzed in other discharges. All profiles, including ones with ordinary Type I, III, or V ELMs were included, unless there was an L-mode phase following the ELM. These "compound ELMs" or "minor disruptions" time slices were excluded because of the large associated dW/dt.

The heat flux profile was measured in NSTX with infrared cameras; the basic method is described here and details are provided elsewhere[10]. The present camera is a commercial 12-bit, 30 Hz micro-bolometer camera with sensitivity in the 8-12 μm range and a measured thermal response time constant of ~ 20ms. The lower divertor tile infrared emission is calibrated during in-situ high temperature bakes, and the heat flux profile is computed from a 1-D conduction model into a semi-infinite solid[11], i.e. neglecting thermal transport along the surface of the tile.

Results – NBI and I_p scan

Figure 1 shows the following quantities vs. P_{loss}: (a) the outer divertor SOL heat flux width mapped to the outer midplane, $\lambda_q^{SOL,mid}$, (b) the outer divertor SOL heat flux width, and $\lambda_q^{SOL,div}$, (c) the outer divertor private-flux region (PFR) heat flux width, $\lambda_q^{PFR,div}$, The mapping of the heat flux profile to the midplane is done by converting the divertor radius to normalized poloidal flux, $\psi_N \equiv (\psi_{axis} - \psi)/(\psi_{axis} - \psi_{sep})$ with an equilibrium reconstruction[12], and computing the midplane equivalent radius at the same ψ_N. Note that the error bars represent the statistics of all of the profiles chosen for analysis from each discharge. The error bars obtained from this method, i.e. from the variability of the individual profiles relative to the mean, are generally larger than the statistical error bars associated with the individual profiles. As commonly observed[4] in NSTX, the inner divertor was partially detached in these discharges, leading to low peak heat flux, and is irrelevant in terms of power flow and peak heat flux. Data for panels (a), (b), and (c) were obtained by fitting the profiles with a standard exponential form. Whereas a single exponential accurately describes the profile on the PFR side, the profile on the SOL side is typically characterized by a rapid decay for the first 2-3 SOL widths, followed by a larger decay length in the far SOL. Most of the power is carried in the first part of the profile near the separatrix, and hence the values plotted correspond to the near SOL. Note that loss power is defined as $P_{LOSS} = P_{OH} + P_{NBI} - dW_{MHD}/dt - P_{rad}^{core} - P_{loss}^{fast\ ion}$, where P_{OH} is the ohmic heating power, P_{rad}^{core} is the core radiated power, and $P_{loss}^{fast\ ion}$ is the fast ion loss. Based on the power accounting study[7], it is assumed that $P_{rad}^{core} \sim 0.1(P_{OH} + P_{NBI})$ and $P_{loss}^{fast\ ion} \sim 0.2(P_{OH} + P_{NBI})$.

Panel 1(a) shows that $\lambda_q^{SOL,mid}$ dropped suddenly near $P_{loss} \sim 3$ MW, but was otherwise relatively independent of P_{loss}. The interpretation is that the divertor transitioned from a nearly detached regime to a high recycling, conduction-limited regime below $P_{loss} \sim 3$ MW, as indicated by the rapid increase in outer divertor peak heat flux[3]. Note that outer divertor partial detachment for $P_{loss} < 3$ MW was ruled out because there was no sign of volume recombination in the D_γ/D_α line emission ratio. Thus, it is difficult to conclude any dependence of $\lambda_q^{SOL,mid}$ on P_{loss} for $P_{loss} \geq 3$ MW. Note also that the discharges reverted back to L-mode at the very lowest P_{LOSS} as it was below the H-L threshold at the operating densities in those discharges.

Panel 1(a) also includes data from three different models[13]. Models D (blue curve) and M (green curve), applicable at high SOL collisionality, give comparable results quantitatively well below the measured widths and have the following dependencies:

$$\lambda_q^{D}[cm] = 0.35 q_{95}^{-0.1} R_m^{0.3} a_m^{0.4} P_{loss}^{-0.4} \quad (1)$$

$$\lambda_q^{M}[cm] = 0.083 q_{95}^{0.6} R_m^{1.0} a_m^{0.4} P_{loss}^{-0.4} \quad (2)$$

Model B1 (red curve), applicable at low SOL collisionality, yields SOL widths comparable to the measured widths and has the following dependencies:

$$\lambda_q^{B1}[cm] = 0.3 q_{95}^{0.73} R_m^{0.27} a_m^{-0.18} P_{loss}^{0.18} B_t^{-0.57} n_{sep}^{-0.18} \quad (3)$$

For these scalings, q_{95} is the safety factor at the 95% flux surface, R_m is the major radius [m], a_m is the minor radius [m], and n_{sep} is the midplane separatrix density [10^{20} m^{-3}]; the units of P_{loss} and B_t are in [MW] and [T] respectively. A final empirical scaling (not shown in panel 1(a)) from a multi-machine analysis[14] is given by:

$$\lambda_q^{AK}[cm] = (2/7)\lambda_{te}^{AK} = 0.088 R_m^{1.0} \quad (4)$$

It can be seen in panel 1(a) that none of the scalings in (1)-(3) seems to capture the characteristics of the NSTX data. Moreover the scaling from (4) implies a fixed SOL width of 0.08cm for NSTX, i.e. well below the values presented in this memo. While model B1 is

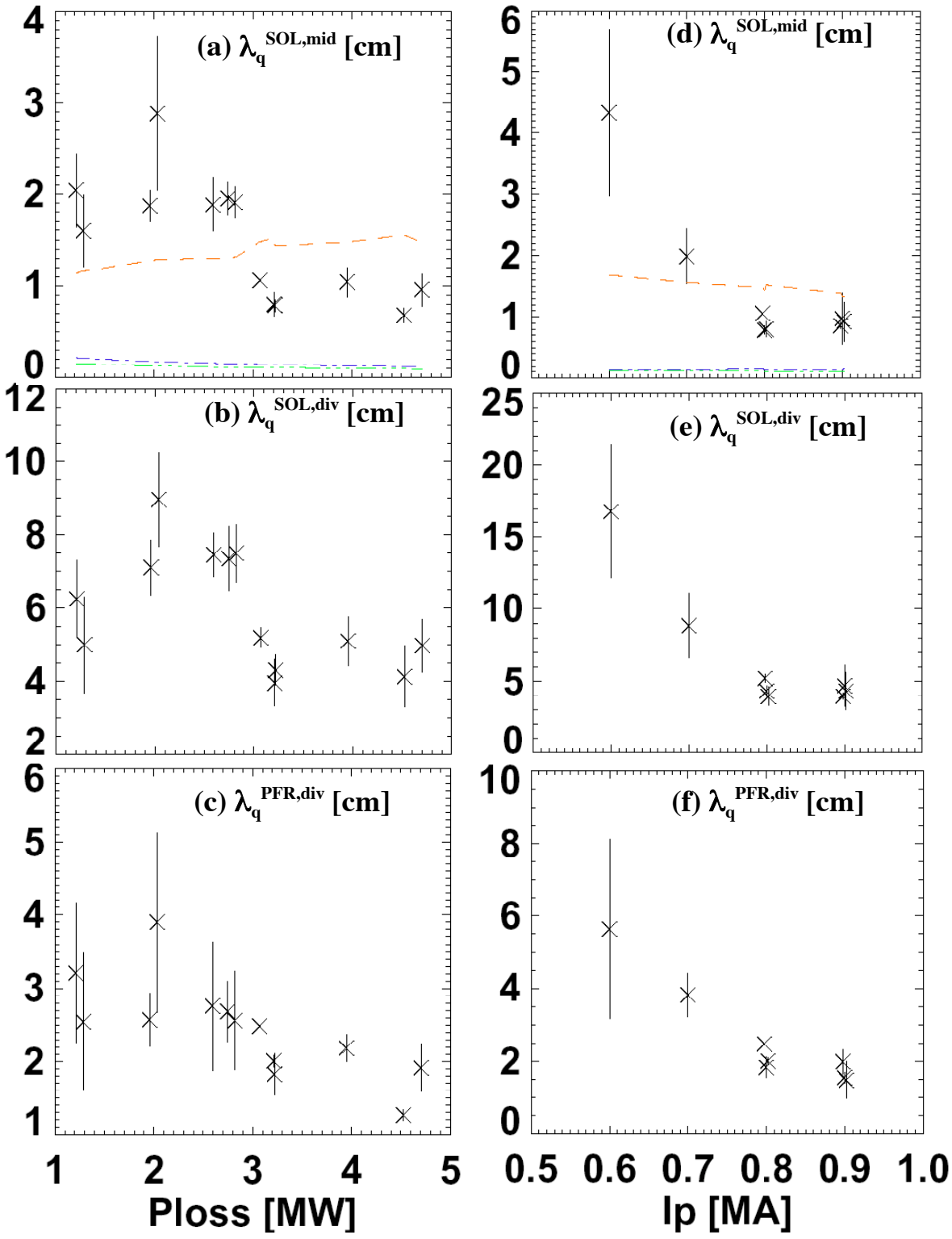

Fig. 1 – (a) midplane, (b) SOL divertor, and (c) PFR divertor heat flux widths vs. P_{loss}, and I_p, (panels d-f), compared with models from equations 1-3.

quantitatively close, the scaling was derived for low collisonality regimes, which is not applicable to the NSTX SOL with collisionality typically between 1 and 100.

Panels 1(d)-(f) show the same quantities defined in panels 1(a)-(c) vs. $I_{p,}$ at fixed P_{NBI} = 4 MW, with 3.0 < P_{loss} < 3.4 MW. Note that B_t was held fixed at 0.45 T during this scan, i.e. q_{95} was varied as well. Panel 1(d) shows a strong apparent inverse dependence of $\lambda_q^{SOL,mid}$ on I_p. Fit to a power law over the entire dataset, $\lambda_q^{SOL, mid} \sim I_p^{-3.8}$, which has strong implications for extrapolation to next step STs. Neglecting the 0.6 MA datapoint solely because it was in a different ELM regime still yields a strong dependence, namely $\lambda_q^{SOL, mid} \sim I_p^{-2.3}$.

Models M and B1 both reflect an inverse relationship between $\lambda_q^{SOL, mid}$ and I_p, owing to the positive q_{95} dependence in the scalings. However the magnitude of the inverse dependence in the data is much stronger than in the models. Note that this inverse dependence may saturate for $I_p \geq 0.8$ MA. It is clear that more data are required to resolve the I_p dependence, particularly in the higher range of I_p, and also at fixed q_{95}.

Conclusions

The midplane SOL heat flux width is relatively insensitive to the SOL loss power when $P_{loss} \geq 3$ MW, and appears to scale inversely with a strong exponent with I_p at fixed P_{loss}. Additional data are required to clarify the I_p and q_{95} dependencies, particularly at high I_p. The experimental values are quantitatively larger than the collisional SOL transport models considered in this memo, and the dependencies differ from scalings of several analytic models. Thus additional work is needed to identify the underlying physics that sets the midplane SOL heat flux width in STs.

Acknowledgements

This research was sponsored in part by the U.S. Dept. of Energy under contracts #DE-AC05-00OR22725 and #DE-AC02-76CH03073. The author acknowledges use of the heat flux analysis code from Charles Lasnier, and discussions with Vlad Soukhanovskii. The efforts of the NSTX plasma operations staff, the neutral beam operations staff, and the computer support staff is gratefully acknowledged.

References

[1] Y.-K. M. Peng, P.J. Fogarty, T.W. Burgess, et. al., *Plasma Physics Controlled Fusion* **47** (2005) B263.

[2] R. Maingi, et. al., *Nuclear Fusion* **43** (2003) 969.

[3] R. Maingi, C.E. Bush, R. Kaita, H.W. Kugel, A.L. Roquemore, S.F. Paul, V.A. Soukhanovskii, and the NSTX team, et. al., *J. Nucl. Materials* **363-365** (2007) 196.

[4] V. A. Soukhanovskii, et. al., *J. Nucl. Materials* **337-339** (2005) 475.

[5] V. A. Soukhanovskii, R. Maingi, R. Raman, R.E. Bell, C. Bush, et. al., *J. Nucl. Materials* **363-365** (2007) 432.

[6] V. A. Soukhanovskii, R. Maingi, R. Raman, R.E. Bell, C. Bush, et. al., *this conference, paper P2.024* (2007).

[7] S. F. Paul, et. al., *J. Nucl. Materials* **337-339** (2005) 251.

[8] A. R. Field, et. al., *Plasma Physics Controlled Fusion* **46** (2004) 981.

[9] R. Maingi, et. al., *Plasma Physics Controlled Fusion* **46** (2004) A305.

[10] D. M. Mastrovito, et. al., *Review of Scientific Instruments* **74** (2003) 5090.

[11] C. J. Lasnier, et. al., *Nuclear Fusion* **38** (1998) 1225.

[12] S. A. Sabbagh, S.M. Kaye, J. Menard, et. al., *Nuclear Fusion* **41** (2001) 1601.

[13] G. F. Counsell, et. al., *Journal of Nuclear Materials* **266-269** (1999) 91.

[14] A. Kallenbach, et. al., *J. Nucl. Materials* **337-339** (2005) 381.